Impact of stain normalization and patch selection on the performance of convolutional neural networks in histological breast and prostate cancer classification

Computer Methods and Programs in Biomedicine Update 1 (2021) 100004

Contents lists available at ScienceDirect

Computer Methods and Programs in Biomedicine Update

journal homepage: www.elsevier.com/locate/cmpbup

Impact of stain normalization and patch selection on the performance of convolutional neural networks in histological breast and prostate cancer classification

Massimo Salvi[a,*], Filippo Molinari[a], U Rajendra Acharya[b,c,d], Luca Molinaro[e], Kristen M. Meiburger[a]

[a] PoliTo^BIO Med Lab, Biolab, Department of Electronics and Telecommunications, Politecnico di Torino, Corso Duca degli Abruzzi 24, Turin 10129, Italy
[b] Department of Electronics and Computer Engineering, Ngee Ann Polytechnic, Singapore
[c] Department of Biomedical Engineering, School of Science and Technology, SUSS University, Clementi 599491, Singapore
[d] Department of Bioinformatics and Medical Engineering, Asia University, Taiwan
[e] A.O.U. Città della Salute e della Scienza Hospital, Division of Pathology, Corso Bramante 88, Turin 10129, Italy

ARTICLE INFO

Keywords:
Convolutional neural networks
Deep learning
Digital pathology
Image analysis
Pre-processing

ABSTRACT

Background: Recently, deep learning has rapidly become the methodology of choice in digital pathology image analysis. However, due to the current challenges of digital pathology (color stain variability, large images, etc.), specific pre-processing steps are required to train a reliable deep learning model.

Method: In this work, there are two main goals: i) present a fully automated pre-processing algorithm for a smart patch selection within histopathological images, and ii) evaluate the impact of the proposed strategy within a deep learning framework for the detection of prostate and breast cancer. The proposed algorithm is specifically designed to extract patches only on informative regions (i.e., high density of nuclei), most likely representative of where cancer can be detected.

Results: Our strategy was developed and tested on 1000 hematoxylin and eosin (H&E) stained images of prostate and breast tissue. By combining a stain normalization step and a segmentation-driven patch extraction, the proposed approach is capable of increasing the performance of a computer-aided diagnosis (CAD) system for the detection of prostate cancer (18.61% accuracy improvement) and breast cancer (17.72% accuracy improvement).

Conclusion: We strongly believe that the integration of the proposed pre-processing steps within deep learning frameworks will allow the achievement of robust and reliable CAD systems. Being based on nuclei detection, this strategy can be easily extended to other glandular tissues (e.g., colon, thyroid, pancreas, etc.) or staining methods (e.g., PAS).

1. Introduction

Digital pathology, in which histology slides are digitized, plays a fundamental role in modern clinical practice. In fact, the analysis of histological slides is crucial for cancer detection and diagnosis, often weighing on expert pathologists who need to review and analyze an immense number of slides for a thorough diagnosis [1]. Due to this large workload, the manual analysis and quantitative grading (e.g., Gleason score) of digital histopathological slides is time consuming and is often affected by a low inter- and intra- operator variability [2,3].

With the onset of whole slide imaging and higher computing power, the application of artificial intelligence, especially convolutional neural networks (CNNs), has grown exponentially over the last few years in the field of digital pathology. In fact, the complexity contained within one high-resolution whole slide image (a common resolution is 100k x 100k) and the presence of color information due to tissue staining make the extraction of important information extremely difficult for human readers [4].

Artificial intelligence and CNNs in particular present numerous advantages to traditional methods, with the capacity of automatically learning high-level features that are useful for disease detection and classification without having to extract handcrafted features [5]. While the potential of using CNNs in medical image analysis is great, particularly in the field of digital pathology, it is also of fundamental importance to feed into the network input data that is representative of the problem

* Corresponding author.
E-mail address: massimo.salvi@polito.it (M. Salvi).

https://doi.org/10.1016/j.cmpbup.2021.100004
Received 18 December 2020; Received in revised form 27 January 2021; Accepted 4 February 2021

that must be solved so as to optimize the potential results. Preparing and optimizing the data for a subsequent algorithm or deep learning model is often referred to as pre-processing. In the field of digital pathology, there are two main preprocessing steps: stain normalization and patch extraction. These two preprocessing steps are used whether the CNN task be classification, detection, or segmentation.

Stain normalization methods modify the colors of the analyzed image by using the chromatic characteristics of a specific target reference image. Numerous studies have shown how including a stain normalization step before inputting the image to a CNN can noticeably increase classification performance in digital pathology [6–8].

Patch extraction, on the other hand, is fundamental in digital pathology as high-resolution patches of the whole slide image (WSI) include the discriminative data that are key for proper classification. Due to this, it is crucial to train the CNN using high-resolution patches and then subsequently predict the label of the entire image using the individual patch predictions. Currently, the mainstream method of patch extraction is simply extracting all patches in a grid-like manner, using a sliding window to extract all patches for CNN training [9,10]. This technique, however, is not optimal for histopathological images, as it is common for the discriminative data to be encrypted only in specific types or areas of tissue. Over the last few years, different segmentation-guided patch extraction methods have also been proposed for digital pathology image analysis [11]. These methods extract the patch only on informative regions (which can be even only a small fraction of the raw image), significantly saving computational resources without sacrificing informative input data and, hence, network performance. However, there is a lack of studies documenting the effect of non-grid patch extraction techniques within deep learning frameworks.

In this paper, we present and evaluate the impact of an automated method for smart patch selection in histopathological images of prostate and breast tissue. The proposed algorithm is specifically designed to extract the patches only on informative regions, most likely representative of where cancer can occur. In the specific cases of breast and prostate cancer, the most representative regions are those with a high density of cell nuclei, whose morphology and texture can be altered during the evolution of the disease. The aim of this work is to evaluate the impact of the proposed strategy within a deep learning framework for the detection of prostate and breast cancer.

2. Materials and methods

In this paper, a deep learning pipeline is presented for cancer detection in histopathological images and its impact is assessed. The proposed strategy consists in three steps: stain normalization, segmentation-guided patch selection and deep network architecture. A detailed description of the algorithm is provided in the next sections.

2.1. Dataset composition

Our dataset consists of 1000 hematoxylin and eosin (H&E) stained images of prostate and breast tissue. Prostate images were collected from an anonymized repository used for teaching purposes at the Division of Pathology, Department of Oncology, Turin, Italy. Digital images were scanned with a magnification of x100 using an Aperio AT2 digital slide scanner. Five images of 1500 × 1500 pixels were extracted from each WSI ($n = 100$), for a total of 500 images. The prostate dataset consisted of 250 healthy images, 33 Stage I, 118 Stage II, 74 Stage III and 25 Stage IV cancers. For each prostate image, the pathologist manually assigned a label: 0 for benign images and 1 for tumoral ones. The dataset was then divided into two subsets: Train set (400 images, 50% healthy) and test set (100 images, 50% healthy).

The breast images were retrieved from the BACH challenge [12]. This challenge consisted in automatically classifying H&E-stained breast images in four classes: 1) Normal, 2) Benign, 3) In situ carcinoma, and 4) Invasive carcinoma. All the images were collected at x200 magnification (conversion factor: 0.467 μm/pixel). Since the aim of this work is to perform a binary classification (healthy vs. tumor), we used the label *Healthy images* for "Normal" (127 images) and "Benign" classes (119 images), while the label *Tumoral images* was employed for all the "In situ carcinoma" (127 images) or "Invasive carcinoma" (127 images). A total of 500 breast histopathological images were used, 400 for training (50% healthy) and 100 for testing the network (46% healthy). Table S1 shows the details of the dataset employed in this work.

2.2. Stain normalization

The first preprocessing step of the proposed pipeline is stain color normalization. A stain normalization method allows transforming an image I into another image I_N, through the operation $I_N = f(I, \alpha)$, where $f(\cdot)$ represents the mapping function that matches the visual appearance of the source image with a predefined template image and α represents a set of chromatic parameters extracted from the template image. Stain normalization represents a crucial step as the appearance of histological stains often suffers from large variability due to the ability of the laboratory technician or the chemical reactions of the dye during the sample preparation [13]. Previous studies have also shown that the standardization of stain intensity plays a crucial role in the development of deep learning solutions for quantitative analysis of histopathological images [14]. Starting from the original RGB image of the specimen (Fig. 1), we applied the normalization strategy described in Ref. [15].

2.3. Segmentation-guided patch selection

This section describes the object detection strategy used to select the informative patches used for training deep networks. First, the proposed strategy applies a segmentation algorithm to detect all the unstained areas and nuclear regions. Since simple thresholding may be ineffective to properly segment all the white areas, our algorithm employs a series of Gabor filters, which are defined as follows:

$$G(x, y, \lambda, \theta, \psi, \sigma, \gamma) = \exp\left(-\frac{x'^2 + \gamma^2 y'^2}{2\sigma^2}\right)\cos\left(\frac{2\pi x'}{\lambda} + \psi\right) \quad (1)$$

where $x' = xcos(\theta) + ysin(\theta)$ and $y' = -xsin(\theta) + ycos(\theta)$. The parameters employed by the Gaussian function are listed in Table S2. Eight directions (θ) are considered to make the algorithm faster and to reduce the noise level. The obtained eight filtered images are thresholded with a value equal to 95% of their maximum. Then, the resulting eight binary masks are merged together with the OR operator (Figure S1).

Cell nuclei are segmented using the blue-ratio (BR) segmentation scheme [16]. The BR image allows highlighting all pixels with a strong blue component, often representative of the hematoxylin-stained areas (i.e., nuclei). The BR image is computed as:

$$BR_{IMAGE} = \frac{100 \times B}{R + G + B} \times \frac{1}{1 + R + G + B} \quad (2)$$

where R, G, and B are the red, green, and blue layers of the normalized image, respectively. After applying min-max scaling to the BR image, the object-based thresholding described in Ref. [17] is employed to obtain a raw binary mask of cell nuclei. Then, all the segmented objects with an area less than 10 μm^2 are deleted as they are too small to be considered as potential nuclei. Finally, a morphological opening with a disk of 3-pixel radius is carried out to obtain smoother contours.

Since the discriminative information are encrypted in high-resolution tiles, a sliding window approach is employed to extract all the relevant patches within the histological tissue. Specifically, a smart patch extraction is adopted that exploits the segmentation masks (nuclei and white) previously identified. All the patches (500 × 500 pixel, 50% overlap) that show a minimum of 15% of nuclei and a maximum of 40% of white areas are selected by the algorithm to train the deep network. In this way, the patches are only extracted from regions with

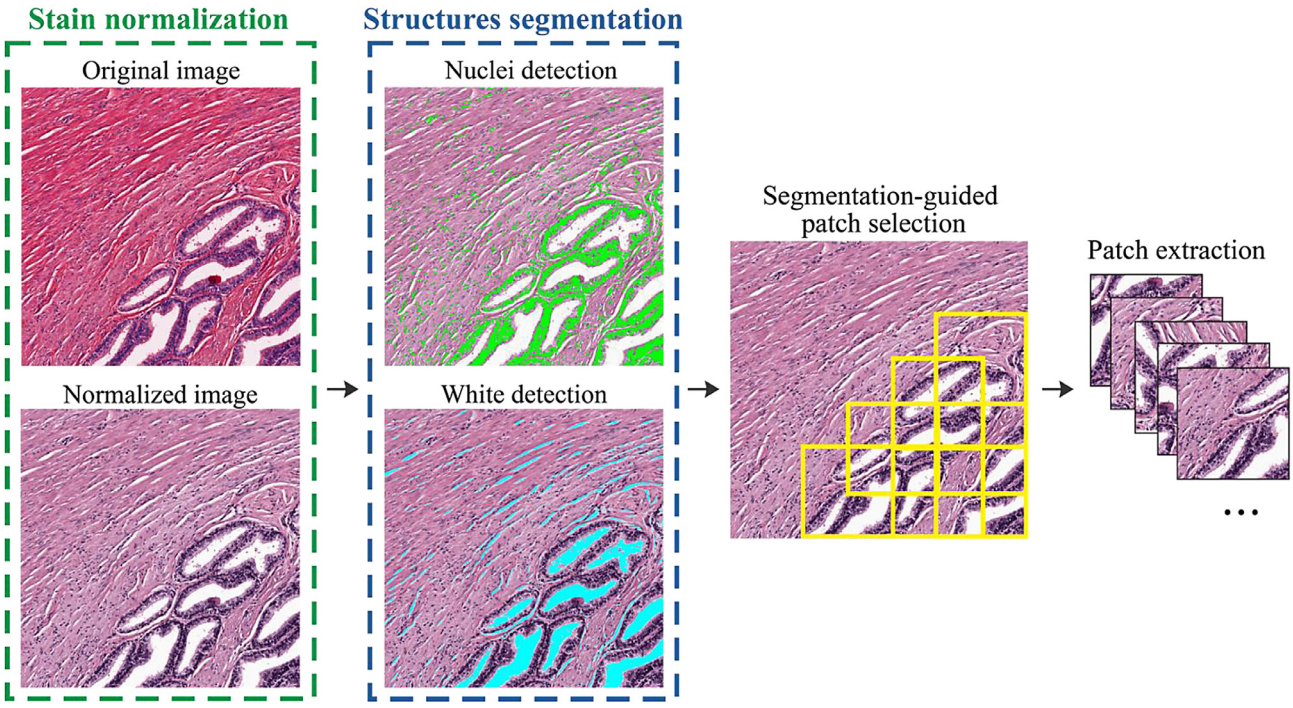

Fig. 1. Schematic representation of the smart patch extraction proposed in this work. Starting from the original RGB image, a preprocessing stage is employed to standardize the staining intensity. Then, cell nuclei and white areas are detected to automatically extract the patches based on local nuclear density.

a high density of nuclei, most likely representative of where cancer can occur. The flowchart of the proposed strategy is illustrated in Fig. 1.

2.4. Deep network architecture

After patch extraction, the proposed pipeline performs tumor detection using a CNN. Specifically, the InceptionV3 architecture [18] is employed for the classification task (Figure S2). This network adopts "Inception" modules that consist in the concatenation of convolutional layers having different kernel sizes to extract multiscale characteristics from the image. The Inceptionv3 is pretrained on ILSVRC 2012 ImageNet [19] and the transfer learning strategy is applied during the network's training in order to overcome the limitations of our limited dataset and to reduce the training time [20,21]. Moreover, on-the-fly data augmentation is implemented by applying random transformations (i.e., flipping, shifting, rotation) to the input images. This strategy prevents network overfitting and makes the model more robust by increasing the amount of data available during training. The deep network is trained with a mini-batch size of 256 and an initial learning rate of 10^{-3}. Binary cross-entropy and the Adam optimizer are employed as a loss and optimization function, respectively. Finally, the total number of epochs is set to 50, with a validation patience of 10 for early stopping of the training process.

2.5. Performance metrics

The overall accuracy of the deep learning model in classifying patches (patch-level accuracy) and in providing the label of the entire image (image-level accuracy) is evaluated by computing the classification accuracy. Sensitivity and specificity of the model are also computed to quantify the fraction of true positive and true negative examples correctly classified by the model. Finally, the ROC curves are calculated to assess the overall performance of the proposed deep learning pipeline.

3. Results

The classification performance provided by our approach (smart extraction from normalized images) is compared with two different strategies: grid extraction from original images and grid extraction from normalized images. In this way, it is possible to isolate the contribution of each pre-processing step within our pipeline (i.e., image normalization and segmentation-guided patch selection). Figs. 2 and 3 show a visual comparison between the three different strategies for a prostate image and a breast image, respectively. The entire processing is performed on a custom workstation with 3.1 GHz octa-core processor and 32-GB of RAM (Turin, Italy).

3.1. Patch-level performance

A quantitative comparison is carried out to assess the performance of the proposed approach for cancer detection. Specifically, the overall accuracy, sensitivity, and specificity of the deep learning model are evaluated in terms of patch classification. Table 1 shows the comparison between our preprocessing strategy and the other two approaches for prostate and breast images. The segmentation-guided patch extraction coupled with the stain normalization strategy showed excellent performance, obtaining an accuracy of over 93% in prostate cancer detection and an accuracy of 84% in breast cancer detection. During the detection of prostate cancer, the proposed strategy improved the performance of the deep network with an increase in accuracy of 22%, sensitivity of 13%, and specificity up to 30% compared to the baseline approach (grid extraction from original images). Similar results were obtained for breast cancer, where the proposed strategy allowed a 17% accuracy improvement compared to the baseline. Moreover, sensitivity increased by 5% while specificity increased by up to 27% with respect to the grid extraction from the original images.

3.2. Image-level performance

During testing, the proposed algorithm extracts all the relevant patches and feeds them into the Inceptionv3 to perform classification. A

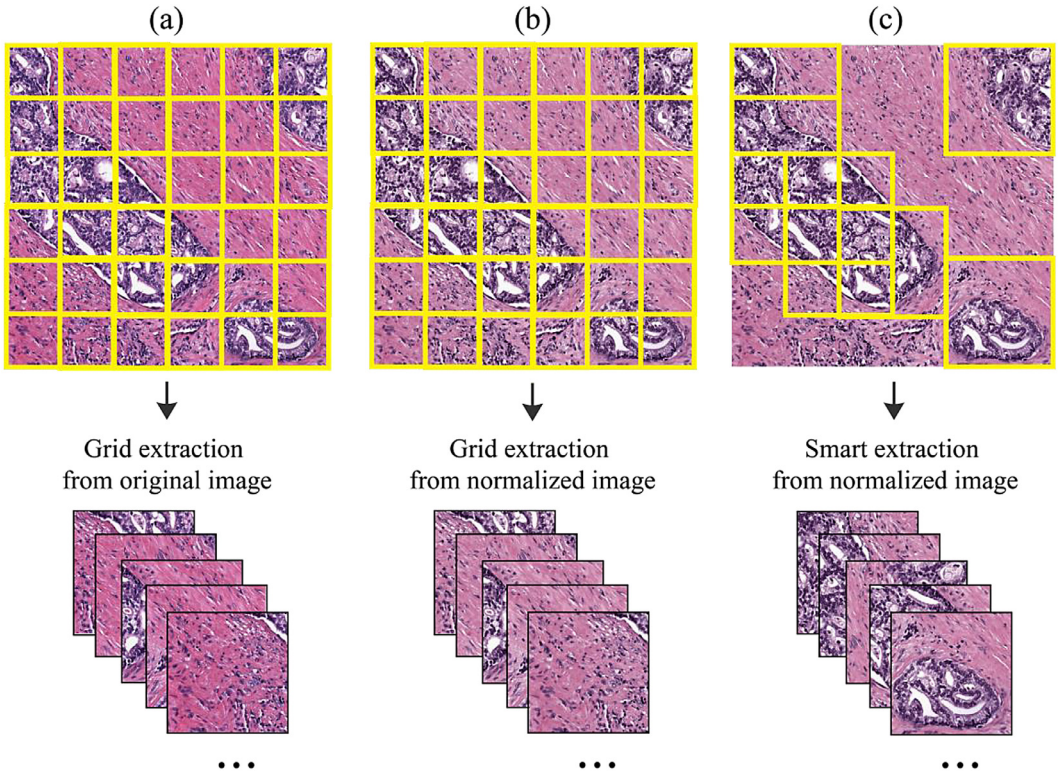

Fig. 2. Visual comparison in patch extraction between three different strategies for a prostate case. (a) patches are selected using a sliding window approach with a 50% overlap on the original image, (b) patches are selected using a sliding window approach with a 50% overlap on the normalized image, (c) patches are selected using an automatic segmentation-driven approach with a 50% overlap on the normalized image.

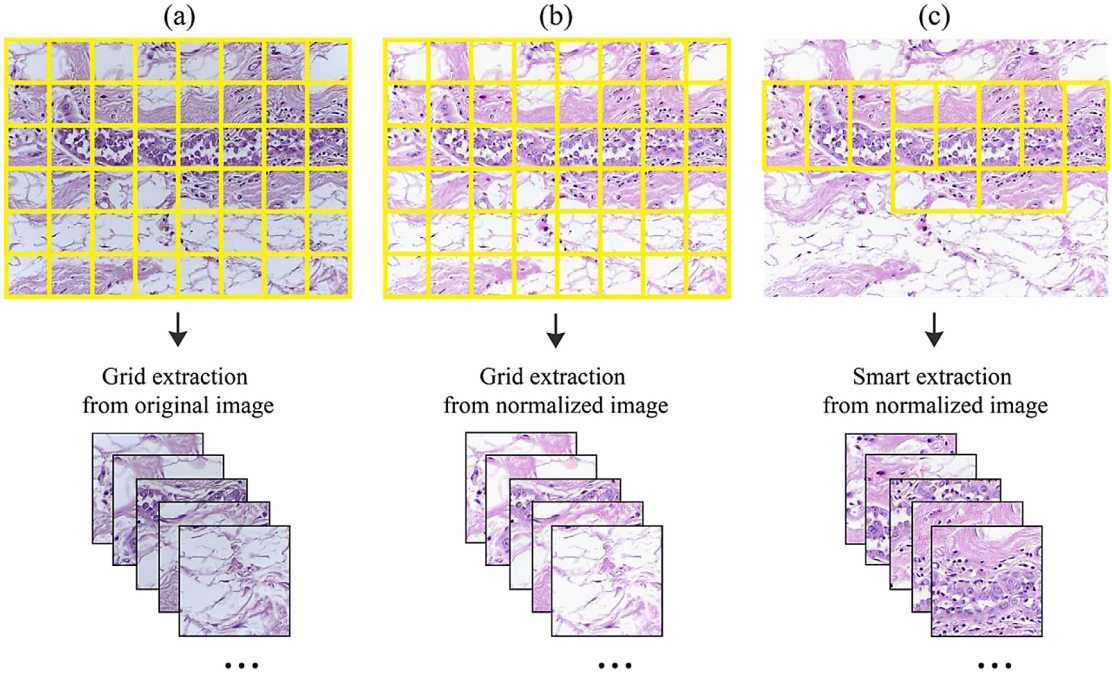

Fig. 3. Visual comparison in patch extraction between three different strategies for a breast case. (a) patches are selected using a sliding window approach with a 50% overlap on the original image, (b) patches are selected using a sliding window approach with a 50% overlap on the normalized image, (c) patches are selected using an automatic segmentation-driven approach with a 50% overlap on the normalized image.

Table 1
Patch-level performance of the proposed method during the classification of prostate and breast cancer.

Pre-processing strategy	Subset	Prostate tissue			Breast tissue		
		Accuracy	Sensitivity	Specificity	Accuracy	Sensitivity	Specificity
Original + grid	Train	0.7123	0.8167	0.6080	0.6714	0.8121	0.5327
sampling	Test	0.7016	0.8288	0.5744	0.6811	0.8651	0.4652
Normalization + grid	Train	0.7977	0.7391	0.8562	0.7199	0.8187	0.6211
sampling	Test	0.7904	0.7456	0.8352	0.7151	0.8259	0.5851
Normalization + smart	Train	0.9386	0.9369	0.9410	0.8422	0.8692	0.8082
sampling	Test	0.9300	0.9530	0.9001	0.7700	0.7327	0.8311

Table 2
Image-level performance of the proposed method during the classification of prostate and breast cancer.

Pre-processing strategy	Subset	Prostate tissue			Breast tissue		
		Accuracy	Sensitivity	Specificity	Accuracy	Sensitivity	Specificity
Original + grid	Train	0.8111	0.9222	0.7000	0.7278	0.8833	0.5722
sampling	Test	0.8100	0.9400	0.6800	0.7300	0.9630	0.4565
Normalization + grid	Train	0.8972	0.8389	0.9556	0.7833	0.9000	0.6667
sampling	Test	0.8600	0.7800	0.9400	0.8100	0.9444	0.6522
Normalization + smart	Train	0.9972	1.000	0.9944	0.9050	0.9000	0.9101
sampling	Test	0.9900	1.000	0.9800	0.8400	0.8519	0.8261

voting procedure is then applied to the patch-level predictions to determine the class of the entire image: the final label of the image is decided by majority voting on the label of classified patches (Figure S3). In other words, the image-level label is equal to the predicted label of the patch with maximum probability over all other patches and classes.

The image-level prediction provided by the algorithm is then compared with the manual label assigned by an expert pathologist. A quantitative comparison is carried out by evaluating the accuracy of the presented method during the classification of prostate and breast cancer. Table 2 shows the performance of the three pre-processing strategies using the train and test subsets, respectively. The confusion matrixes of the compared methods are reported in Table S3. The combination of stain normalization and smart patch selection allowed to reach 100% sensitivity and almost 100% accuracy and specificity for prostate cancer. Our preprocessing strategy also outperformed the compared methods for breast cancer detection, obtaining an overall accuracy of 90%. In addition, as occurred for patch-level performance, our approach has resulted in improved image-level performance in terms of both sensitivity and specificity, showing at most a 2% and 33% increase, respectively.

Figure S4 illustrates the ROC curves obtained during prostate and breast cancer detection for each of the three pre-processing strategies. A detailed description of the ROC curves is reported in the Supplementary Material. The extraction of patches from normalized images allows to increase the area under the curve (AUC) for both tumor types. Starting with the same extraction strategy (grid sampling), a 6% increase in AUC for prostate cancer detection and a 5% improvement in AUC for breast images were observed. Even more interesting, the segmentation-driven patch selection allowed to further increase the AUC of the deep network, reaching 1.0 for prostate cancer and 0.97 for breast cancer.

4. Discussion and conclusions

While CNNs are still sometimes viewed as a black box that does not explain predictions in a manner that is easily understandable by humans, one fact remains true: the input data is of pivotal importance. If the network receives non-informative data as input, the final performance of the network can only be compromised [10,22]. In light of this, data curation and preprocessing techniques are fundamental to properly prepare the data for the network that can then be trained to its maximum potential.

In this study, we present a fully automated pre-processing strategy for the smart selection of the informative patches inside histopathological images of prostate and breast tissue, and assess its impact on the final network's performance. By combining a stain normalization step and a segmentation-driven patch extraction, our approach is capable of increasing the performance of a CAD system designed for prostate and breast cancer detection.

Our data curation and preprocessing strategy was compared with two common strategies: grid extraction from the original images and grid extraction from normalized images. Many previous studies have shown the benefits from using stain normalization before implementing a deep learning framework. As expected, by simply inserting the stain normalization step before classifying each patch, the overall accuracy of the deep learning model increased, both in terms of single-patch performance and of image-level performance (Tables 1 and 2).

While the impact of stain normalization is duly detailed in literature, there are not nearly as many studies documenting the impact of non-grid techniques of patch extraction. Hence, in this study, the impact of the proposed patch selection on the deep learning model has been investigated. The increase in accuracy, sensitivity and specificity using a smart patch extraction is greater than the improvement that was observed by implementing only stain normalization. The combination of stain normalization and smart patch selection allows to increase both the sensitivity (false negative reduction) and specificity (false positive reduction) of the deep learning model. In particular, integrating stain normalization with a smart segmentation-driven patch selection gave forth an accuracy of 99% (AUC = 1.0) for prostate cancer and 90% (AUC = 0.97) for breast cancer. These results demonstrate that the selection of representative patches has a great impact on the training of a deep learning model for digital pathology image analysis. In fact, a targeted extraction of patches allows the training of the network only on informative regions, which in the case of breast and prostate cancer, is where neoplasm could be potentially manifested.

In this work, we present a simple yet effective pipeline for smart patch extraction in histopathological images of prostate and breast tissue. Being based on nuclei detection, this strategy can be easily extended to other glandular tissues (e.g., colon, thyroid, pancreas, etc.) or staining methods (e.g., PAS). In addition, we are planning to extend our dataset with images acquired from multiple centers and with different scanners to further increase the robustness of the algorithm. Our research group is currently working on an extension of the proposed method for the analysis of entire prostate biopsies, with the aim of developing an accurate and reliable tool for prostate cancer screening. We also plan to implement a classifier specifically designed to distinguish between benign areas and early-stage tumors, which still represents a challenge for both pathologists and machine learning models.

Declaration of Competing Interest

The authors declare that they have no known competing financial interests or personal relationships that could have appeared to influence the work reported in this paper.

Supplementary materials

Supplementary material associated with this article can be found, in the online version, at doi:10.1016/j.cmpbup.2021.100004.

References

[1] S. Al-Janabi, A. Huisman, P.J. Van Diest, Digital pathology: current status and future perspectives, Histopathology 61 (2012) 1–9.

[2] M.J. van den Bent, Interobserver variation of the histopathological diagnosis in clinical trials on glioma: a clinician's perspective, Acta Neuropathol. 120 (2010) 297–304.

[3] D.R.J. Snead, Y. Tsang, A. Meskiri, P.K. Kimani, R. Crossman, N.M. Rajpoot, E. Blessing, K. Chen, K. Gopalakrishnan, P. Matthews, Validation of digital pathology imaging for primary histopathological diagnosis, Histopathology 68 (2016) 1063–1072.

[4] M.K.K. Niazi, A.V. Parwani, M.N. Gurcan, Digital pathology and artificial intelligence, Lancet Oncol. 20 (2019) e253–e261.

[5] A. Janowczyk, A. Madabhushi, Deep learning for digital pathology image analysis: a comprehensive tutorial with selected use cases, J. Pathol. Inform. 7 (2016) 29, doi:10.4103/2153-3539.186902.

[6] C. Chen, Y. Huang, P. Fang, C. Liang, R. Chang, A computer-aided diagnosis system for differentiation and delineation of malignant regions on whole-slide prostate histopathology image using spatial statistics and multidimensional DenseNet, Med. Phys. 47 (2020) 1021–1033.

[7] A. Anghel, M. Stanisavljevic, S. Andani, N. Papandreou, J.H. Rüschoff, P. Wild, M. Gabrani, H. Pozidis, A high-performance system for robust stain normalization of whole-slide images in histopathology, Front. Med. 6 (2019) 193–205.

[8] H. Cho, S. Lim, G. Choi, H. Min, Neural stain-style transfer learning using gan for histopathological images, ArXiv Prepr. 80 (2017) 1–10. ArXiv1710.08543.

[9] P. Ambrosini, E. Hollemans, C.F. Kweldam, G.J.L.H. van Leenders, S. Stallinga, F. Vos, Automated detection of cribriform growth patterns in prostate histology images, ArXiv Prepr. 10 (2020) 1–13 ArXiv2003.10543.

[10] H.S. Ryu, M.-S. Jin, J.H. Park, S. Lee, J. Cho, S. Oh, T.-Y. Kwak, J.I. Woo, Y. Mun, S.W. Kim, Automated gleason scoring and tumor quantification in prostate core needle biopsy images using deep neural networks and its comparison with pathologist-based assessment, Cancers 11 (2019) 1860.

[11] A. Golatkar, D. Anand, A. Sethi, Classification of breast cancer histology using deep learning, in: Proceedings of the International Conference on Image Analysis and Recognition, Springer, 2018, pp. 837–844.

[12] G. Aresta, T. Araújo, S. Kwok, S.S. Chennamsetty, M. Safwan, V. Alex, B. Marami, M. Prastawa, M. Chan, M. Donovan, Bach: grand challenge on breast cancer histology images, Med. Image Anal. 56 (2019) 122–139.

[13] T.A.A. Tosta, P.R. de Faria, L.A. Neves, M.Z. do Nascimento, Computational normalization of H&E-stained histological images: progress, challenges and future potential, Artif. Intell. Med. 95 (2019) 118–132.

[14] Y. Zheng, Z. Jiang, H. Zhang, F. Xie, J. Shi, C. Xue, Adaptive color deconvolution for histological WSI normalization, Comput. Methods Programs Biomed. 170 (2019) 107–120.

[15] M. Salvi, N. Michielli, F. Molinari, Stain Color Adaptive Normalization (SCAN) algorithm: separation and standardization of histological stains in digital pathology, Comput. Methods Programs Biomed. 193 (2020) 105506.

[16] H. Chang, L.A. Loss, B. Parvin, Nuclear segmentation in H&E sections via multi-reference graph cut (MRGC), in: Proceedings of the IEEE International Symposium on Biomedical Imaging, 2012.

[17] M. Salvi, F. Molinari, Multi-tissue and multi-scale approach for nuclei segmentation in H&E stained images, Biomed. Eng. Online. (2018) 17, doi:10.1186/s12938-018-0518-0.

[18] C. Szegedy, V. Vanhoucke, S. Ioffe, J. Shlens, Z. Wojna, Rethinking the inception architecture for computer vision, in: Proceedings of the IEEE Conference on Computer Vision and Pattern Recognition, 2016, pp. 2818–2826.

[19] A. Krizhevsky, I. Sutskever, G.E. Hinton, Imagenet classification with deep convolutional neural networks, in: Proceedings of the Advances in Neural Information Processing Systems, 2012, pp. 1097–1105.

[20] D. Sarkar, R. Bali, T. Ghosh, Hands-On Transfer Learning With Python: Implement advanced Deep Learning and Neural Network Models Using TensorFlow and Keras, Packt Publishing Ltd, 2018.

[21] S. Saxena, S. Shukla, M. Gyanchandani, Pre-trained convolutional neural networks as feature extractors for diagnosis of breast cancer using histopathology, Int. J. Imaging Syst. Technol. (2020).

[22] A. Cruz-Roa, H. Gilmore, A. Basavanhally, M. Feldman, S. Ganesan, N.N.C. Shih, J. Tomaszewski, F.A. González, A. Madabhushi, Accurate and reproducible invasive breast cancer detection in whole-slide images: a Deep Learning approach for quantifying tumor extent, Sci. Rep. 7 (2017) 46450.